Power Absorption in Laser-Sustained Argon Plasmas

Dennis Keefer,* Richard Welle,† and Carroll Peters‡
The University of Tennessee Space Institute, Tullahoma, Tennessee

In this experimental investigation, stable and axisymmetric laser-sustained plasmas were produced in flowing argon. Energy was provided by the focused beam from a carbon dioxide laser; two different focusing geometries were used. Spatial distributions of absolute radiance from the plasmas, in a narrow-wavelength band, were measured. The assumption of axial symmetry, along with the assumption of local thermodynamic equilibrium, was used to deduce the radial profiles of temperature in the plasmas. From this and a geometric raytrace, the detailed spatial distribution of power absorption was calculated, as well as the radiation lost from the plasmas. In addition to the focusing geometry, the flow velocity, pressure, and incident laser power were systematically varied in the experiments. The quantitative results indicate clearly that a perceptive analysis of such laser-sustained plasmas must take into consideration the two-dimensionality of both the flowfield and the laser energy distribution in the focused beam.

Introduction

IT has been proposed[1,2] that the absorption of a high-energy laser beam in a laser-sustained plasma (LSP) could be utilized to provide a rocket propulsion system of exceptionally high specific impulse. The laser beam power would be absorbed by the electrons in a very high-temperature (15,000–20,000 K) plasma through inverse bremsstrahlung, as opposed to direct absorption by molecular species. The practical realization of such a system requires creation of an LSP with two essential characteristics: stability in the presence of a forced convective flow, and nearly complete absorption of the laser beam power. In addition, the plasma will have to be sustained in a flow in which mixing occurs between the extremely high-temperature plasma core and an outer buffer flow. This mixing is required to ensure a nearly uniform flow of propellent at temperatures sufficiently high to provide the required specific impulse, but at temperatures low enough to ensure survival of the nozzle.[3]

Some experimental studies of the LSP have been carried out in previous investigations,[4-6] however, none of these were performed in a forced convective flow environment. Several effects of the flow environment are critical for LSP use in a propulsion system: the effect on plasma stability, fractional absorption of the laser beam, and the required focusing optics. Several previous studies have shown that the LSP is stable for only certain finite combinations of plasma pressure and laser power.[4,7,8] However, the effect of convective flow and focusing geometry was not studied systematically.

The first theoretical investigation was carried out by Raizer,[9] who relied heavily on the similarity with the physics of subsonic combustion. Several one-dimensional analyses of the LSP followed in the spirit of the Raizer analysis,[10-12] but used more sophisticated analytical and computational methods. None of these analyses is capable of addressing the important two-dimensional aspects of the focusing of laser beam energy and radial flow. A simplified model was proposed which considered the two-dimensional effects of thermal conduction but did not include the effects of radial flow or beam focusing.[13,14] Recently, Gulati and Merkle[15] and Merkle[16] developed numerical techniques capable of treating the full two-dimensional problem. The use of the LSP for propulsion has recently been reviewed by Glumb and Krier.[17]

In this paper, some results of the first systematic attempt to study the LSP in a controlled convective flow are reported. The plasmas were created in flowing argon within a cylindrical quartz chamber using a relatively low-power (1.5-kW) carbon dioxide laser operated at a 10.6-μm wavelength. Argon was chosen because it is relatively easy to create the LSP in argon with the available laser power, and spectroscopic diagnosis of argon plasmas is relatively straightforward. Experiments were conducted using two different focusing geometries, pressures of 1.3–2.3 atm, a range of subsonic flow velocities, and incident power levels from 360 to 840 W.

To understand the detailed physical processes occurring within the LSP, it is desirable to measure the temperature field within the high-temperature plasma. In a high-temperature plasma which can be considered in local thermodynamic equilibrium (LTE), laser beam absorption, and thermal and radiation transport depend only on the plasma temperature and pressure. Thus, if the detailed temperature field is known the spatial dependence of these processes can be determined. In this experiment, the detailed temperature field was measured by recording digital images of the plasma through a narrow-bandpass filter which was chosen to isolate a portion of the continuum radiation from the plasma. The data acquisition system was calibrated to measure the absolute radiance of the plasma emission; using the assumption of LTE, this measurement can be related to the plasma temperature. Once the temperature field has been measured, the detailed power absorption and loss within the plasma can, in principle, be calculated.

Experimental Procedure

The LSP was produced using a plano-convex focusing lens and entrance window of sodium chloride (NaCl) in a cylindrical quartz flow tube having a converging entrance section. The laser power was provided by a 1.5-kW, continuous-wave (cw), axial-flow, electric discharge carbon dioxide laser using a relatively low-magnification (1.5) unstable oscillator. This produces an annular output beam having excellent axial symme-

Presented as Paper 85-1552 at the AIAA 18th Fluid Dynamics, Plasmadynamics and Lasers Conference, Cincinnati, OH, July 16-18, 1985; received Sept. 9, 1985; revision received Feb. 24, 1986.

*Professor, Engineering Science and Mechanics, The Center for Laser Applications. Member AIAA.

†Pre-Doctoral Fellow, The Center for Laser Applications. Student Member AIAA.

‡Professor, Mechanical and Aerospace Engineering, The Center for Laser Applications. Member AIAA.

try, which is highly desirable to ensure the axial symmetry of the plasma required for accurate plasma diagnostics. Axial symmetry of the plasma was also aided by operating the flow chamber with the optical and chamber axes vertical, so that nonaxisymmetric effects induced by buoyancy were eliminated. The experimental apparatus is shown in Fig. 1, and is described in more detail in Ref. 18.

Laser power was monitored by use of a NaCl wedge placed in the output beam to split off a fraction of the beam and direct it into a laser power meter. The system was calibrated using a calibrated power meter whose capacity was adequate to accept the entire output power from the laser.

The argon flow was introduced radially through a screen into a 74-mm-diam inner quartz tube which converged smoothly to a 22-mm-diam cylindrical test section. In all cases, the plasma was contained within the cylindrical test section. The inner flow tube was contained within an outer cylindrical quartz tube which contained the chamber pressure. The outer tube was closed on the downstream end by a water-cooled copper cone which absorbed the transmitted beam energy and cooled the heated flow downstream of the plasma.

Focusing lenses of both 8- and 12-in. focal length were used to sustain plasmas with somewhat different results. A detailed geometric raytracing analysis of the optical system consisting of both the lens and the window indicated that spherical aberration limits the intensity at focus, and that the peak intensity was greater with the 12-in. lens. The raytrace analysis also showed that the intensity distribution in the unabsorbed annular beam along the optical axis in the focal region was different for the two lenses.

The intensity at focus of the laser beam, for the cw laser used in these experiments, is insufficient to initiate gas breakdown, therefore, an alternative technique was used to initiate the plasma. A 2.5-mm-diam tungsten rod, commonly used for TIG welding, was inserted axially into the focal volume of the lens. Laser heating of the tungsten liberates sufficient electrons through thermionic emission to initiate a plasma which is sustained by the process of inverse bremsstrahlung absorption of the laser beam. Once the plasma was initiated the tungsten rod was withdrawn downstream along the optical axis. When a stable plasma was achieved, the chamber pressure, flow rate, and laser power were set to the desired values and the required digital images of the plasma emission were acquired. The pressure, flow rate, and laser power could then be set to new conditions without reinitiation of the plasma. The process was repeated until the required data had been obtained.

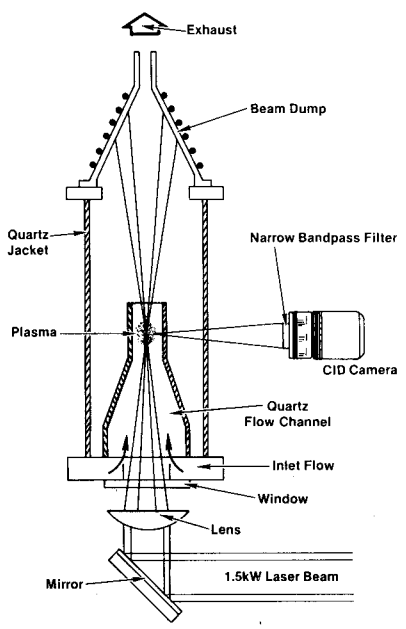

Fig. 1 Experimental apparatus.

The primary measurements acquired from the experiments were digital images of the plasma. These images were obtained by a CID (charge injection device) video camera whose spectral range was limited by a narrow-bandpass interference filter. The filter was chosen to isolate a 1-nm-wide region of the continuum radiation from the plasma, free of line radiation. For the argon plasma, the filter was centered at 626.5 nm. The digital images were acquired using a VICOM image processing computer, which allowed images to be acquired at video frame rates (60/s) and averaged into memory. The entire image acquisition system was calibrated through direct substitution of a standard lamp of spectral radiance. Since the experiment was designed to ensure axial symmetry of the plasma, the image intensity could be Abel-inverted to provide spatially resolved measurements of the plasma emission coefficient. The plasma emission coefficient could then be related to the plasma temperature, for an LTE plasma, through theoretical calculations verified by measurements in arc plasmas.[19]

Data Reduction and Analysis

The digital images of the plasma contained 512 × 240 pixels obtained from single field scans of the camera. Typically, 16 of these images were averaged into memory to improve the signal-to-noise ratio in the low-intensity outer edges of the plasma image. The camera background signal was then subtracted from this image and the image was subsampled axially to provide the data used in the Abel inversion. Each radial scan, which was obtained at approximately 0.5-mm intervals along the axis of the plasma, contained approximately 70 points. For reference, the maximum diameter of the 10,000 K isotherm is approximately 6 mm.

Images of the standard lamp filament, taken through the narrow-bandpass filter and calibrated neutral density filters, were used to obtain absolute values for the plasma radiance, and images of graph paper, taken through the quartz flow tube, were used to obtain the spatial calibration of the system. The location of the focal spot within the camera image field was estimated, with the laser operating at reduced power, by adjusting the tungsten rod along the optical axis and noting the point at which maximum brightness occurred.

The centerline of the plasma image was determined by finding, for each radial scan, the fold point of minimum variance and then computing the least-squares best-fit straight line for this set of minimum variance points. Each radial scan was then folded about this centerline and fitted, in a least-squares sense, to a series of cubic splines which were then Abel-inverted to obtain the emission coefficient.[20] When the emission coefficient had been calculated, the temperature was obtained, for the pressure appropriate to the experiment,

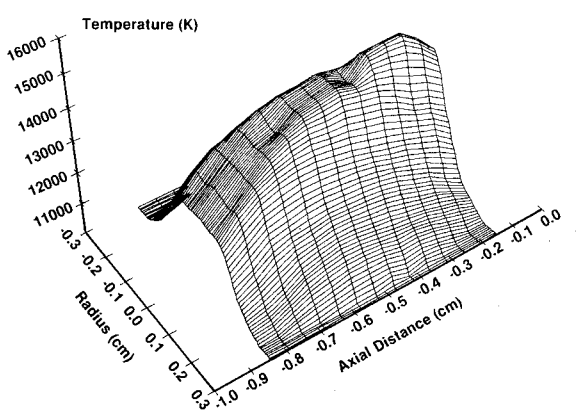

Fig. 2 Three-dimensional representation of the temperature field for a 2-atm argon plasma sustained using an 8-in. focal length lens.

by interpolation in the tabulated data published by Morris and Yos.[19] To illustrate the typical results obtained, a three-dimensional representation of the temperature field for a plasma sustained using the 8-in. focusing lens at a nominal pressure of 2 atm of argon is shown in Fig. 2.

The overall accuracy of this measurement technique is influenced by several factors: absolute radiometric calibration of the optical system, spatial calibration of the image, optical distortion due to the quartz envelope, the accuracy of the Abel inversion, and the validity of the data used to relate plasma temperature and the emission coefficient. Of these factors, the most important appears to be the distortion produced by the quartz envelope, as evidenced by the dip in measured plasma temperature seen in Fig. 2 at an axial distance of −0.4 cm. This effect can, in principle, be removed by careful calibration of each pixel in the digital image. Another factor was a change in the absolute calibration during one experimental series due to coating of the quartz wall, as observed during runs 206–211. These effects are most noticeable in the higher temperature regions of the plasma where the change of the emission coefficient with temperature is small, and may result in errors in peak temperature of 10%. The effect of these errors on the other computed quantities, such as the laser absorption coefficient, is mitigated somewhat by the fact that they are also relatively weak functions of temperature near the maximum temperature measured in these experiments.

In order to calculate the power absorption within the plasma, a grid system was defined to contain the plasma; at each grid point a value of absorption coefficient at 10.6 μm was calculated from the measured temperature field. The method used for this calculation was described by Kemp and Lewis.[21] The required thermodynamic properties of argon plasmas have been tabulated by Drellishak et al.,[22] and the Gaunt factors were published by Karzas and Latter.[23] The incoming laser beam was divided into a finite number of rays, each representing a discrete fraction of the total power of the laser, such that, when summed, the total would approximate the beam profile of the laser. Each of these rays was traced geometrically through the focusing optics and grid system, and at each step the power absorption was calculated. The absorbed power was then subtracted from the ray and added to the appropriate location in a corresponding grid of power absorption. The power remaining in each ray was summed to obtain the total power transmitted and, from that, the total power absorbed in the plasma. Figure 3 is a three-dimensional representation of the power absorption in the plasma of Fig. 2. In tracing each ray through the plasma, the assumption was made that the path would not be significantly affected by the gradient in the refractive index. Subsequent analysis, utilizing the procedure described by Cheng and Casperson,[24] indicates that any given ray may be deflected up to a maximum of 200 μm from a straight path. The resulting error in total calculated power absorption is less than 5% and depends on the position of the plasma relative to the focal point of the incident laser beam. In addition, the effects of diffraction, which are of this same order, have been neglected.

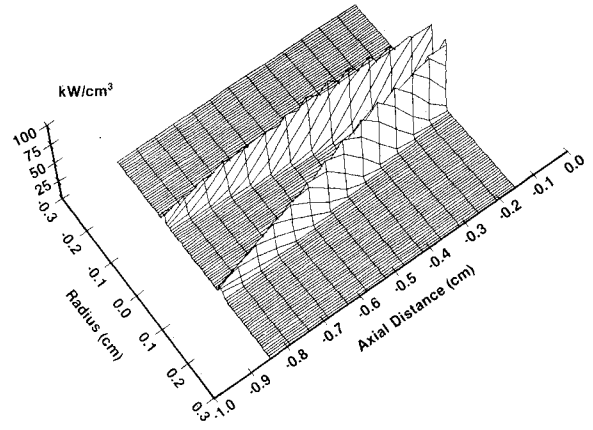

Fig. 3 Three-dimensional representation of the spatial distribution of laser power absorption in the plasma of Fig. 2.

Radiation loss as a function of position was calculated from the temperature field according to the relation published by Kozlov et al.[25] for optically thin radiation. Resulting values were integrated numerically over the volume to obtain the radiation loss from the plasma. Figure 4 shows a three-dimensional representation of the total radiation loss field of the plasma of Fig. 2.

Experimental Results

The initial objective of this study was to investigate the effect of a forced convective flow on the LSP. Figure 5 shows a sequence of four isotherm plots of plasmas sustained at a nominal pressure of 2 atm in argon, an incident laser power of 710 W using the 8-in. focal length lens, and average upstream flow rates from 0.36 to 6.46 std. liters/min, corresponding, at 2-atm pressure, to approach velocities of 0.8-15 cm/s. (The

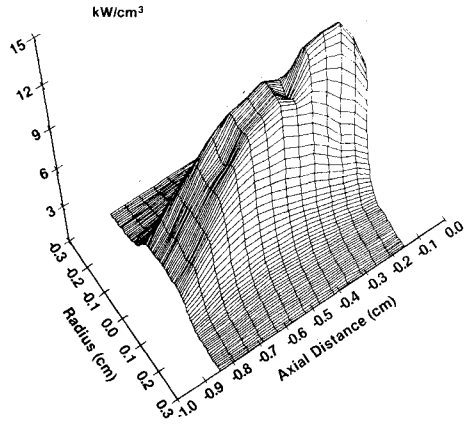

Fig. 4 Three-dimensional representation of the radiative power loss field for the plasma of Fig. 2.

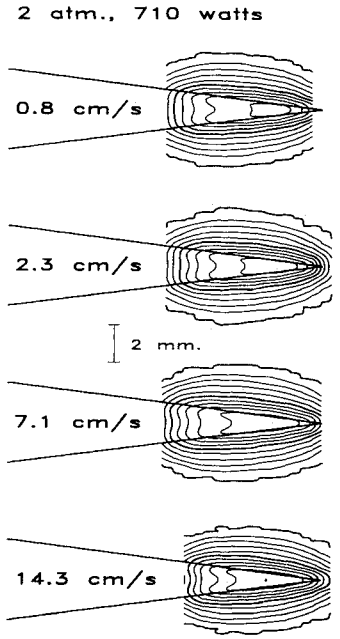

Fig. 5 Sequence of isothermal contour plots showing the effect of changing the flow rate in the plasma test chamber, while holding constant the pressure and laser power. The contour interval is 500 K; the outer contour is at 10,000 K.

contour interval in this and all subsequent plots is 500 K, with the outer contour at 10,000 K.) The principal effect of increasing the flow in this range is to move the plasma somewhat nearer the focal point. The plasma was stable at all flow conditions, and the maximum velocity used represents a limit imposed by the available flowmeter. Figure 6 is a graph of the fractional power absorption as a function of flow rate for this set of plasmas. Reference to this graph and plasma numbers 202–205 in Table 1 shows that an order-of-magnitude change in flow rate had a negligible effect on both the fractional power absorption and the maximum temperature of the plasma, while the increase in flow rate caused a slight decrease in the fraction of absorbed power that was lost as radiation.

A similar sequence of contour plots, shown in Fig. 7, illustrates the variation of the plasma shape and size in response to the incident laser power. In this sequence, the flow rate and pressure were held constant as the laser power was reduced. (In running the experiment, the plasma was extinguished and had to be reinitiated between runs 205 and 206, and it appears that there was some change in calibration factor at this time, possibly due to coating of the quartz during initiation. As a result, the measured peak temperatures of all the succeeding plasmas were lower than the earlier runs. In particular, plasmas 000, 204, and 208 were run at identical conditions, and while the peak temperatures of 000 and 204 are comparable, that of 208 appears to be lower by 1000 K. However, while the absolute numbers are uncertain, the trends are still thought to be significant.) The effect of reducing the incident power is to reduce the plasma volume and to confine the plasma in a region nearer the focal point. This suggests that the plasma expands into the beam until it reaches a point where the laser intensity falls below some threshold value, and the previous sequence indicates that the threshold value depends weakly on the incident flow velocity. Fractional power absorption as a function of incident power is graphed in Fig. 8, and is tabulated, along with fractional radiation loss and peak temperature for plasmas 207–211, in Table 1. From these, it is seen that decreasing the incident laser power results in a slight decrease in both fractional power absorption and fractional radiation loss, while at the same time there is a slight increase in the maximum plasma temperature, possibly due to concentration of the plasma in the region of highest incident laser intensity.

Plasma pressure and the lens focal length also have a significant effect on the plasma shape and size. Another sequence of plasma isotherm contour plots is shown in Fig. 9, where the plasma pressure was varied while holding the incident laser power constant at a value of 710 W, and the flow constant at a value of 3.2 std. liters/min. These plasmas were

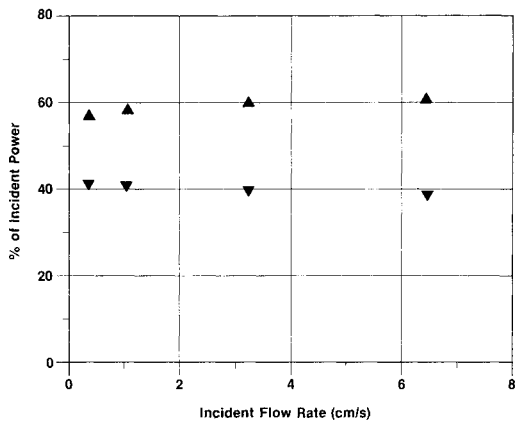

Fig. 6 Variation in fractional power absorption (▲) and radiation loss (▼) with a changing flow rate. The pressure and laser power are held constant in this series.

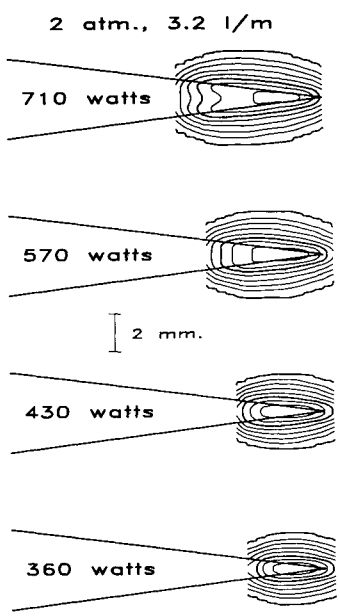

Fig. 7 Sequence of isothermal contour plots showing the effect of changing the incident laser power while holding the pressure and flow rate constant.

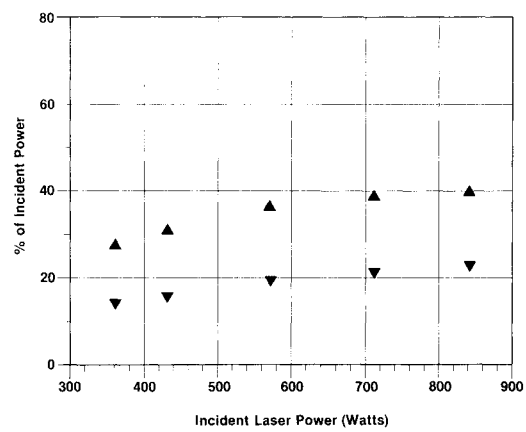

Fig. 8 Variation in fractional power absorption (▲) and radiation loss (▼) with changing incident laser power, at constant pressure and flow rate.

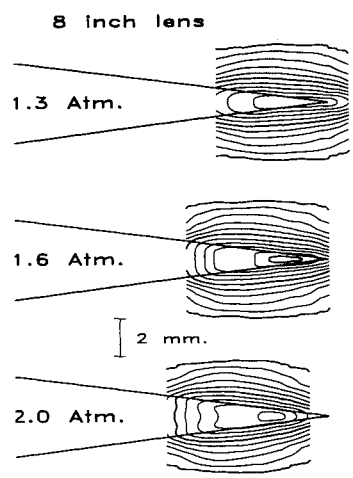

Fig. 9 Isothermal contour plots of plasmas sustained using the 8-in. focal length lens, showing the effect of changing the chamber pressure while holding constant the mass flow rate and incident laser power.

Table 1 Summary of measured and calculated properties of argon plasmas sustained in this experiment

Plasma no.	Pressure, atm	Flow rate, cm/s	Incident power, W	Power absorbed,[a] % of incident	Power radiated,[a] % of absorbed	Peak temperature, K
000	1.97	7.2	710	51	80	14,700
001	1.65	8.6	710	52	73	15,300
002	1.31	10.8	710	42	64	15,100
003	2.33	6.1	637	40	82	14,100
004	1.97	21.5	710	50	75	14,700
005	1.65	25.6	710	52	67	15,100
006	1.31	32.3	710	41	61	15,000
007	2.33	18.1	710	44	73	14,200
100	1.31	10.8	710	47	73	14,900
101	1.65	8.6	710	41	77	14,400
102	1.97	7.2	710	23	79	13,400
202	1.98	0.8	710	57	72	14,700
203	1.98	2.3	710	58	70	14,900
204	1.98	7.1	710	60	66	14,900
205	1.98	14.3	710	61	63	15,000
206	1.98	21.4	710	41	52	13,800
207	1.98	7.1	840	40	57	13,500
208	1.98	7.1	710	38	56	13,700
209	1.98	7.1	570	36	53	13,800
210	1.98	7.1	430	31	51	13,900
211	1.98	7.1	360	27	52	13,900

[a]Values calculated from measured temperature field.

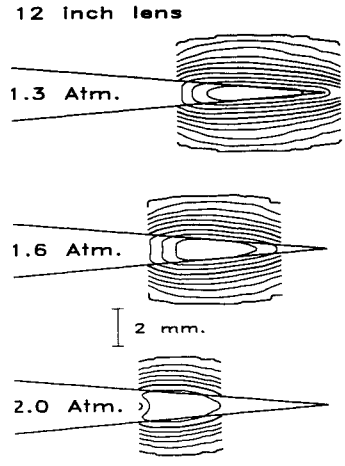

Fig. 10 Isothermal contour plots of plasmas sustained using the 12-in. lens under pressure; flow rate and power conditions identical to those of Fig. 9.

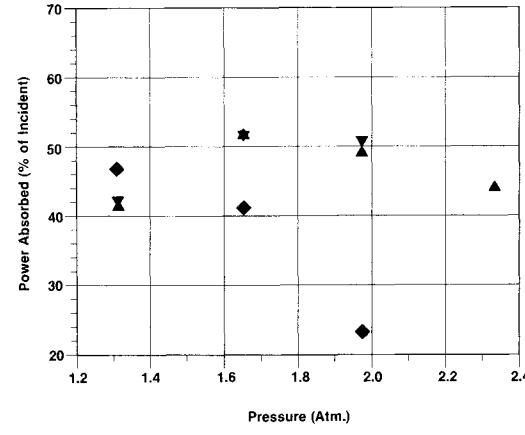

Fig. 11 Change in fractional power absorption with changing pressure for three sets of plasmas: 8-in. lens, 3.2 std. liters/min (▲); 8-in. lens, 9.6 std. liters/min (▼); 12-in. lens, 3.2 std. liters/min (◆); all at 710 W incident laser power.

sustained with the 8-in. focal length lens. Accompanying this, in Fig. 10, is a sequence of isotherm contour plots for plasmas sustained with the 12-in. lens at identical power, flow, and pressure values. Figure 11 is a graph of fractional power absorption vs pressure for these two sequences and a third sequence in which the plasmas were sustained with the 8-in. lens at 710 W and a flow rate of 9.6 std. liters/min. For the sequence with the 8-in. lens at 3.2 std. liters/min, the plasma moves upstream as the pressure increases, while both the fractional power absorption and fractional loss decrease. The temperature maximum occurs at the intermediate pressure value. Similar results are observed for the 12-in. focal length lens, but the behavior is shifted to a lower pressure. Indeed, using the longer focal length lens, the plasma could not be initiated at 2-atm pressure, but ignited readily at 1.3 atm, and could be sustained while increasing the pressure to, but not beyond, 2 atm. At this pressure value, the fractional power absorption was the lowest calculated for any of the sustained plasmas herein. Figure 12 is a three-dimensional representation of the power absorption field for this case. By comparison with Fig. 3, which is for a plasma at the same pressure, power, and flow rate, but sustained with the 8-in. lens, it is seen that the plasma in this last case stabilized farther upstream in the converging beam.

The influence of the lens focal length is complicated by the effects of spherical aberrations. Figure 13 shows computer-generated raytraces of the incident beams in the focal region of the 8- and 12-in. lens. The rays are spaced such that each represents 5% of the power present in the measured cylindrical laser beam profile. The raytraces indicate that, because of spherical aberration, the intensity at focus is considerably greater for the 12-in. lens, and a region of relatively high intensity occurs 5–8 mm before the focus in both lenses, due to an annular convergence of the spherically aberrated rays. There is a possibility that the threshold intensity may be reached in either of two places, and this complicates the interpretation of plasma position as a function of the flow and pressure.

The complex beam intensity distribution also complicates the calculation of absorbed power within the plasma. The experimental method used to determine the position of the plasma relative to the focus of the lens will be affected by the distribution near focus; in one case, it was found that a 1-mm

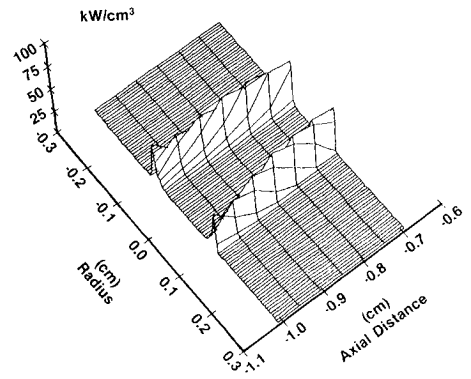

Fig. 12 Three-dimensional representation of the spatial distribution of laser power absorption in a 2-atm plasma sustained using the 12-in. focal length lens, with an incident power of 710 W and a flow rate of 3.2 std. liters/min.

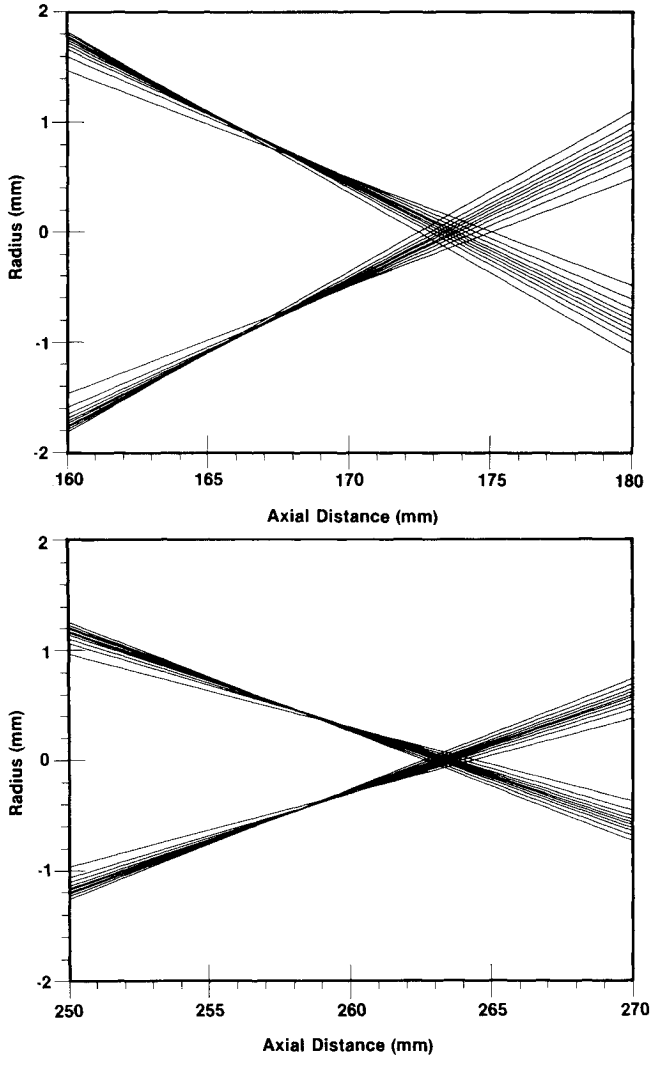

Fig. 13 Ray traces showing the distribution of energy in the focal region of the 8-in. (top) and 12-in. (bottom) focal length lens. The laser beam is incident from the left.

change in the focal position resulted in a change in the calculated fractional power absorption from 54 to 60%.

Discussion and Concluding Remarks

Spatially resolved experimental measurements of plasma temperature, laser power absorption, and thermal radiation loss have been obtained for several laser-sustained plasmas (LSP) in flowing argon. By systematically varying the pressure, flow rate, incident laser power, and focusing geometry of the incident laser beam, it was possible to determine the effect of these parameters on the fraction of incident laser power absorbed by the plasma and on the fraction of absorbed power lost by thermal radiation.

The effect of a forced convective flow is smaller than might have been expected, and primarily consists of forcing the plasma to stabilize at a position a little closer to the focal plane, but with little change in the plasma shape, size, peak temperature, power absorption, or radiation loss characteristics. This suggests that increasing the flow through the plasma may increase the plasma maintenance threshold intensity, but the effect appears small and will require further analysis because of the aberrations in the focal region. It should be noted that the range of flow speeds investigated in this experiment is of the same order of magnitude as the flow occurring as a result of convective accelerations over the length of the plasma. Therefore, it is possible that another order-of-magnitude increase in incident flow speed will have a more significant effect on plasma properties. In the range of speeds investigated, there was no indication that increased flow rate had a destabilizing influence on the plasma; this suggests that the LSP may be suitable for use as a clean, high-temperature gas heater.

Except for the small increase in peak temperature shown in Table 1, the effect of decreasing the incident laser power was about as expected. The upstream surface of the plasma receded to a position closer to the focal plane as the power was reduced, seeking a position of threshold intensity. In addition, decreasing the size of the plasma resulted in a decreased power absorption efficiency, and a slight decrease in the fraction of the absorbed power lost as radiation.

The sensitivity of the plasma to pressure, as seen in Figs. 9–11, is to be expected, since the plasma absorption coefficient is such a strong function of pressure. On the other hand, the strong effect of focusing geometry, as seen in Fig. 11, is somewhat surprising. The two sequences of plasmas operated at 710 W and 3.2 std. liters/min, both show that the power absorption efficiency reaches a maximum at some value of pressure and then decreases as the pressure is further increased, but the pressure at which the maximum occurred was lower for the longer focal length lens. Indeed, it was not possible to initiate the plasma at a pressure of 2 atm using the longer focal length lens, but it could be initiated and sustained easily at 1.3 atm. This was unexpected since examination of Fig. 13 shows that the intensity at the focal plane of the longer focal length lens is considerably greater. Previous experimental studies have attempted to define regions of pressure and power where the plasma could be sustained.[4,7,8] In view of the authors' observations, it would appear that these results should be interpreted as applying only to the specific optical system used for the experiments.

Comparison of the power absorption and the temperature distributions in the plasmas, for these experiments utilizing the annular output from an unstable oscillator, reveals that the power is absorbed in a thin conical region near the outer edges of the plasma. This results in off-axis peaks in plasma temperature in the upstream plasma regions. The use of a Gaussian incident beam profile likely would result in a considerably different temperature field, and might have a significant effect on the fractional power absorption and thermal radiation loss when compared to those observed in these experiments.

The foregoing results underscore the fact that the LSP is strongly affected by the detailed spatial distribution of laser intensity in the focal region. Any attempt to analyze the complex, coupled, nonlinear phenomena in the laser-sustained plasma, either experimentally or analytically, must include the spatial details of the interactions in order to succeed in revealing the true nature of the overall process.

Acknowledgments

The authors gratefully acknowledge the contributions of Newton Wright, Fred Schwartz, and Jim White Jr. in the

design, construction, and operation of the experimental apparatus. This work was supported by the U.S. Air Force Office of Scientific Research; Program Manager, Dr. L. Caveny.

References

[1]Kantrowitz, A.R., "The Relevance of Space," *Astronautics & Aeronautics*, Vol. 9, March 1971, pp. 34-35.

[2]Minovitch, M.A., "Reactorless Nuclear Propulsion—The Laser Rocket," AIAA Paper 72-1095, Dec. 1972.

[3]Keefer, D., Elkins, R., Peters, C., and Jones, L., "Laser Thermal Propulsion," *Orbit-Raising and Maneuvering Propulsion: Research Status and Needs*, Vol. 89, edited by L.H. Caveny, *Progress in Astronautics and Aeronautics*, AIAA, New York, 1984, pp. 129-148.

[4]Generalov, N.A., Ziniakov, V.P., Kozlov, G.I., Masyukov, V.A., and Raizer, Y.P., "Experimental Investigation of a Continuous Optical Discharge," *Soviet Physics-JETP*, Vol. 34, 1972, pp. 763-769.

[5]Klosterman, E.L. and Byron, S.R., "Measurement of Subsonic Laser Absorption Wave Propagation Characteristics at 10.6 Micrometers," *Journal of Applied Physics*, Vol. 45, 1974, pp. 4751-4759.

[6]Keefer, D.R., Henriksen, B.B., and Braerman, W.F., "Experimental Study of a Stationary Laser-Sustained Air Plasma," *Journal of Applied Physics*, Vol. 46, March 1975, pp. 1080-1083.

[7]Moody, C.D., "Maintenance of a Gas Breakdown in Argon Using 10.6 Micrometer CW Radiation," *Journal of Applied Physics*, Vol. 46, June 1975, pp. 2475-2482.

[8]Kozlov, G.I., Kuznetsov, V.A., and Masyukov, V.A., "Sustained Optical Discharges in Molecular Gases," *Soviet Physics-Technical Physics*, Vol. 49, Nov. 1979, pp. 1283-1287.

[9]Raizer, Y.P., "Subsonic Propagation of a Light Spark and Threshold Conditions for the Maintenance of Plasma by Radiation," *Soviet Physics-JETP*, Vol. 31, Dec. 1970, pp. 1148-1154.

[10]Jackson, J.P. and Nielsen, P.E., "Role of Radiative Transport in the Propagation of Laser-Supported Combustion Waves," *AIAA Journal*, Vol. 12, Nov. 1974, pp. 1498-1501.

[11]Kemp, N.H. and Root, R.G., "Analytical Study of Laser-Supported Combustion Waves in Hydrogen," *Journal of Energy*, Vol. 3, Jan./Feb. 1979, pp. 40-49.

[12]Keefer, D.R., Peters, C.E., and Crowder, H.L., "A Reexamination of the Laser Supported Combustion Wave," *AIAA Journal*, Vol. 23, Aug. 1985, pp. 1208-1212.

[13]Batteh, J.H. and Keefer, D.R., "Two-Dimensional Generalization of Raizer's Analysis for the Subsonic Propagation of Laser Sparks," *IEEE Transactions on Plasma Science*, Vol. PS-2, Sept. 1974, pp. 122-129.

[14]Keefer, D.R., Crowder, H.L., and Elkins, R., "A Two-Dimensional Model of the Hydrogen Plasma for a Laser Powered Rocket," AIAA Paper 82-0404, Jan. 1982.

[15]Gulati, A., and Merkle, C.L., "Absorption of Electromagnetic Radiation in an Advanced Propulsion System," *Journal of Spacecraft and Rockets*, Vol. 21, Jan./Feb. 1984, pp. 101-107.

[16]Merkle, C.L., "Prediction of the Flowfield in Laser Propulsion Devices," *AIAA Journal*, Vol. 22, Aug. 1984, pp. 1101-1107.

[17]Glumb, R.J. and Krier, H., "Concepts and Status of Laser-Supported Rocket Propulsion," *Journal of Spacecraft and Rockets*, Vol. 21, Jan./Feb. 1984, pp. 70-79.

[18]Keefer, D.R., Crowder, H.L., and Peters, C.E., "Laser Sustained Argon Plasmas in a Forced Convection Flow," AIAA Paper 85-0388, Jan. 1985.

[19]Morris, J.C. and Yos, J.M., "Radiation Studies of Arc Heated Plasmas," ARL 71-0317, 1971.

[20]Shelby, R.T. and Limbaugh, C.C., "Smoothing Technique and Variance Propagation for Abel Inversion of Scattered Data," AEDC-TR-76-163, 1977.

[21]Kemp, N.H. and Lewis, P.F., "Laser-Heated Thruster Interim Report," NASA CR-161665 (PSI TR-205), Feb. 1980.

[22]Drellishak, K.S., Aeschliman, D.P., and Cambel, A.B., "Tables of Thermodynamic Properties of Argon, Nitrogen, and Oxygen Plasmas," AEDC-TR-64-12, 1964, pp. 167-212.

[23]Karzas, W.J. and Latter, R., "Electron Radiative Transitions in a Coulomb Field," *The Astrophysical Journal, Supplement Series, Supplement No. 55*, Vol. VI, May 1961.

[24]Cheng, T.K. and Casperson, L.W., "Plasma Diagnosis by Laser Beam Scanning," *Journal of Applied Physics*, Vol. 46, May 1975, pp. 1961-1965.

[25]Kozlov, G.I., Kuznetsov, V.A., and Masyukov, V.A., "Radiative Losses by Argon Plasma and the Emissive Model of a Continuous Optical Discharge," *Soviet Physics-JETP*, Vol. 39, No. 3, Sept. 1974, pp. 463-468.